remote sensing

MDPI

Article

Trends of Key Greenhouse Gases as Measured in 2009–2022 at the FTIR Station of St. Petersburg State University

Maria Makarova [1,*], Anatoly Poberovskii [1], Alexander Polyakov [1], Khamud H. Imkhasin [1], Dmitry Ionov [1], Boris Makarov [1,2], Vladimir Kostsov [1], Stefani Foka [1] and Evgeny Abakumov [3]

[1] Department of Atmospheric Physics, Saint Petersburg State University, 7/9 Universitetskaya nab., Saint Petersburg 199034, Russia
[2] Federal State Unitary Enterprise "Alexandrov Research Institute of Technology", Sosnovy Bor 188540, Russia
[3] Department of Applied Ecology, Saint Petersburg State University, 7/9 Universitetskaya nab., Saint Petersburg 199034, Russia
* Correspondence: m.makarova@spbu.ru

Abstract: Key long-lived greenhouse gases (CO_2, CH_4, and N_2O) are perhaps among the best-studied components of the Earth's atmosphere today; however, attempts to predict or explain trends or even shorter-term variations of these trace gases are not always successful. Infrared spectroscopy is a recognized technique for the ground-based long-term monitoring of the gaseous composition of the atmosphere. The current paper is focused on the analysis of new data on CO_2, CH4, and N_2O total columns (TCs) retrieved from high resolution IR solar spectra acquired during 2009–2022 at the NDACC atmospheric monitoring station of St. Petersburg State University (STP station, 59.88°N, 29.83°E, 20 m asl.). The paper provides information on the FTIR system (Fourier-transform infrared) installed at the STP station, and an overview of techniques used for the CO_2, CH_4, and N_2O retrievals. Trends of key greenhouse gases and their confidence levels were evaluated using an original approach which combines the Lomb–Scargle method with the cross-validation and bootstrapping techniques. As a result, the following fourteen-year (2009–2022) trends of TCs have been revealed: (0.56 ± 0.01) % yr^{-1} for CO_2; (0.46 ± 0.02) % yr^{-1} for CH_4; (0.28 ± 0.01) % yr^{-1} for N_2O. A comparison with trends based on the EMAC numerical modeling data was carried out. The trends of greenhouse gases observed at the STP site are consistent with the results of the in situ monitoring performed at the same geographical location, and with the independent estimates of the global volume mixing ratio growth rates obtained by the GAW network and the NOAA Global Monitoring Laboratory. There is reasonable agreement between the CH_4 and N_2O TC trends for 2009–2019, which have been derived from FTIR measurements at three locations: the STP site, Izaña Observatory and the University of Toronto Atmospheric Observatory.

Keywords: trends of greenhouse gases; methane; carbon dioxide; nitrous oxide; remote sensing; atmospheric FTIR observations

Citation: Makarova, M.; Poberovskii, A.; Polyakov, A.; Imkhasin, K.H.; Ionov, D.; Makarov, B.; Kostsov, V.; Foka, S.; Abakumov, E. Trends of Key Greenhouse Gases as Measured in 2009–2022 at the FTIR Station of St. Petersburg State University. *Remote Sens.* **2024**, *16*, 1996. https://doi.org/10.3390/rs16111996

Academic Editors: Tatiana Zhuravleva and Alexander Kokhanovsky

Received: 26 March 2024
Revised: 16 May 2024
Accepted: 28 May 2024
Published: 31 May 2024

1. Introduction

Carbon dioxide (CO_2), methane (CH_4), and nitrous oxide (N_2O) are the key long-lived greenhouse gases (LLGHGs), which have contributed to about 89% of the increase in global radiative forcing from the pre-industrial times [1]. Radiative forcing by LLGHGs increased by 49% from 1990 to 2021, with carbon dioxide accounting for about 80% of that increase [2]. An analysis of the latest data from the GAW WMO (Global Atmosphere Watch, the World Meteorological Organization) observational network revealed that the mixing ratios of carbon dioxide, methane and nitrous oxide in the atmosphere continue to reach the new maximums. The globally averaged surface mixing ratios of LLGHGs observed in 2021 amounted to 415.7 ± 0.2 ppm, 1908 ± 2 ppb, 334.5 ± 0.1 ppb for CO_2, CH_4,

and N_2O, respectively [1]. These three greenhouse gases are perhaps among the best-studied components of the Earth's atmosphere today [3]. Basic information on their importance, atmospheric lifetime and major global sources and sinks is given in Table 1. Although most sources and sinks of LLGHGs are known, their relative contributions to the atmospheric concentrations of LLGHGs still have significant uncertainty, and attempts to predict or explain observed trends or even shorter-period variations of these gases are not always successful [1,4–9]. According to NOAA's GML ESRL data, global growth rates of both CO_2 and N_2O have shown a steady increase since the 1960s and the 2000s (https://gml.noaa.gov/ccgg/trends/gl_gr.html; https://gml.noaa.gov/ccgg/trends_n2o/, accessed on 23 March 2024). At the same time, for CH_4, the dependence of the growth rate on time has a more complex character: the positive values in the 1980s and in the 1990s were replaced by almost zero or even negative values in the 2000s, and then an increase in the CH_4 growth rate started again in 2007–2008 (https://gml.noaa.gov/ccgg/trends_ch4/, accessed on 23 March 2024). For CO_2, the period of 2012–2021 was the decade of highest growth rate since the 1960s, with the maximum values of 2.95 and 2.84 ppmv/year recorded in 2015 and 2016, respectively (https://gml.noaa.gov/ccgg/trends/gl_gr.html, accessed on 23 March 2024) [10,11]. The main cause of this growth is assumed to be the El Niño phenomenon, the third most powerful since the 1950s (Patra et al., 2017). At present, however, it is not always possible to confidently separate the contribution to the accelerating growth of LLGHGs in the atmosphere from natural phenomena and from anthropogenic sources. One of the main reasons, as indicated by Patra et al., 2017 [7], is the uncertainty of trends in anthropogenic regional emissions. Reducing these uncertainties requires not only up-to-date "bottom-up" emission inventories and state-of-the-art chemistry and climate models, but also reliable verified greenhouse gas observing systems which track long-term changes in atmospheric LLGHGs. Additionally, it is necessary to evaluate "top-down" emissions through inverse modelling. In addition to the above-mentioned WMO GAW network, which performs in situ measurements of greenhouse gas concentrations, the following ground-based and satellite remote observational systems are actively used now: TCCON (Total Carbon Column Observing Network, http://www.tccon.caltech.edu/, accessed on 23 March 2024), COCCON (COllaborative Carbon Column Observing Network, https://www.imk-asf.kit.edu/english/COCCON.php, accessed on 23 March 2024), NDACC (Network for the Detection of Atmospheric Composition Change, https://www.ndacc.org, accessed on 23 March 2024) and GOSAT (Greenhouse gases Observing SATellite, https://www.gosat.nies.go.jp, accessed on 23 March 2024), IASI (Infrared Atmospheric Sounding Interferometer, https://www.esa.int/Applications/Observing_the_Earth/Meteorological_missions/MetOp/About_IASI, accessed on 23 March 2024), OCO-2/3 (The Orbiting Carbon Observatory 2/3, https://ocov2.jpl.nasa.gov and https://ocov3.jpl.nasa.gov, accessed on 23 March 2024), TROPOMI (TROPOspheric Monitoring Instrument, https://www.tropomi.eu, accessed on 23 March 2024). It should be noted that the observations of TCCON, COCCON, and NDACC networks are the core element of validation of satellite measurements [12–15].

This paper is devoted to the analysis of the results of the FTIR (Fourier-transform infrared) measurements of the main three greenhouse gases (CO_2, CH_4, and N_2O), which have been carried out since 2009 at the atmospheric monitoring station of St. Petersburg State University (STP station). The main goal of the study is to evaluate a long–term trend of the atmospheric total column of key greenhouse gases for a midlatitude station located on the Baltic Sea coast. In order to achieve this goal, the following research problems were solved:

- the adaptation of retrieval strategies for deriving the total columns of CO_2, CH_4 and N_2O by FTIR spectra of direct solar radiation has been carried out. During this step, special attention was paid to the specific features of the SPbU FTIR system and the weather/climatic conditions of the STP station;

- the archives of FTIR spectra recorded at the STP station within the period 2009–2022 were processed, and these activities resulted in obtaining the fourteen-year series of TCs of key greenhouse gases;
- to evaluate the long-term trend of CO_2, CH_4 and N_2O, an original approach for approximation of the TCs time series has been proposed and implemented. It is based on the Lomb–Scargle harmonic analysis of uneven time series, a cross-validation technique for analyzing the optimality of the fitting model and statistical bootstrapping for evaluating the reliability of the obtained long-term trends

The structure of our article is as follows:

- Introduction;
- Section 1: general information on the SPbU atmospheric monitoring station including geographical, climate and weather features;
- Section 2: a description of the FTIR system installed at the STP station, and an overview of the inverse methods and retrieval strategies used to derive the total columns/profiles of the target gases;
- Section 3: Results and Discussion, including the characterization of the retrieval results and a time series analysis aimed at identifying long-term trends for LLGHG total columns;
- Conclusions.

Table 1. General information on investigated long-lived greenhouse gases (GHGs).

Chemical Formula and Name	Importance	Atmospheric Lifetime	Main Global Sources and Sinks
CH_4, methane	Long-lived GHG, responsible for 16% of the radiative forcing, Global Warming Potential (100 years) GWP = 27–30 [3,16]; CH_4 decay leads to the formation of tropospheric O_3 and stratospheric H_2O [1]	9–12 years [1,17]	Sources: natural wetlands, agriculture and waste, fossil fuels, biomass burning [5]; 50–65% of total emissions come from human activities [3]. Sinks: chemical loss by OH oxidation, soil uptake [5]
CO_2, carbon dioxide	Most abundant long-lived GHG, responsible for 66% of the radiative forcing, GWP = 1, [1,3,16]	Complex function of geochemical and biological processes [17], can reach hundreds of years [18]	Sources: decomposition, ocean release and respiration, fossil fuel combustion, cement production, deforestation and other land-use change (land clearing for agriculture, degradation of soils) [9,17]; ~10% of total emissions come from human activities [19]. Sinks: oceans and land ecosystems [9]
N_2O, nitrous oxide	Long-lived GHG, responsible for 7% of the radiative forcing [1], GWP = 273 [3,16]; stratospheric ozone-depleting substance	116 ± 9 years [6]	Sources: oceans, soils, agriculture, fossil fuel and industry, biomass burning [6]; ~43% of total emissions come from human activities [1]. Sinks: chemical destruction in the stratosphere (by reaction with light and excited oxygen atoms), soils uptake [6]

General Information about the SPbU Atmospheric Monitoring Station

The atmospheric monitoring station of SPbU is a mid-latitude observational station located at 59.88°N, 29.83°E, 20 m asl. It was established in the 1970s (https://phys.spbu.ru/englishpages/history.html, accessed on 23 March 2024) by the efforts of Saint Petersburg State University (former Leningrad State University). In 2016, the

atmospheric monitoring station of SPbU joined the NDACC network [20] as the St. Petersburg site (https://www.ndaccdemo.org/stations/st-petersburg-russian-federation, accessed on 23 March 2024). The instruments for atmospheric monitoring are installed in the suburban Peterhof campus of SPbU, which is located at a distance of ~35 km southwest from the center of St. Petersburg. The geographic location of the observational site of SPbU is indicated on the map in Figure 1 .

St. Petersburg is the second largest city in Russia and the fourth largest city in Europe. According to the official information, the population of St. Petersburg reached ~5.6 million in 2023 (http://council.gov.ru/en/structure/regions/SPE/, accessed on 23 March 2024). The climate of St. Petersburg and its suburbs is classified as humid continental (Dfb—Köppen climate classification) with moderately mild winters and moderately warm summers (http://www.pogodaiklimat.ru/climate/26063.htm, accessed on 23 March 2024, in Russian). The air masses coming from the Atlantic have the greatest influence on the climate of the region. Highly variable weather, with the frequent changes of Polar and Arctic air masses, is largely defined by cyclonic activity. On average, the winds of the western, north-western and south-western directions represent almost 46% (in autumn—about 50%) of all winds. Due to the predominance of westerly winds, most of the observations at the monitoring station are performed outside the St. Petersburg pollution plume and represent a regional background. In addition to FTIR observations, cases of air pollution from both anthropogenic and natural emissions [21] can be detected at the STP station using the NO_2 DOAS measurements [22] as well as in situ monitoring of NO_x, O_3, CO, CH_4 and CO_2 concentrations in the ambient air [23–25]. Mostly, these observational facilities are provided and maintained by the GEOMODEL Resource Center of the SPbU Research Park (https://researchpark.spbu.ru/en/geomodel-eng, accessed on 23 March 2024).

Figure 1. The geographic location of the atmospheric monitoring site of SPbU (St. Petersburg site of the NDACC) is indicated on the map by the red circle. STP is the NDACC acronym for St. Petersburg site.

2. Instruments and Methods

2.1. SPbU FTIR System

In January 2009, ground-based Fourier-transform infrared observations of direct solar radiation in the mid infrared (MIR) spectral region had been started in testing mode at the St. Petersburg site (SPbU). Routine FTIR measurements were launched in March 2009. In 2016, the FTIR system operated by the Atmospheric Physics Department was certified as an IRWG (the Infrared Working Group) NDACC instrument (https://www.ndacc-demo.org/stations/st-petersburg-russian-federation, accessed on 23 March 2024).

The high spectral resolution FTIR system [26,27] replaced the low resolution (~0.4–0.6 cm^{-1}) solar IR dispersive (grating) spectrometer used at the St. Petersburg site in 1991–2009 for total column (TC) measurements of CH_4 and CO [28,29].

The FTIR system is installed in the building of the Faculty of Physics of SPbU. It consists of a commercial Bruker IFS 125HR Fourier transform spectrometer (FTS) with a maximum spectral resolution $\Delta\nu = 0.0019$ cm^{-1} and a self-designed solar tracker developed and assembled at the Atmospheric Physics Department of SPbU [30]. The FTS and precise positioning sensor of solar tracker are placed in an air-conditioned room. The Bruker IFS 125HR is equipped with LN-cooled InSb and MCT detectors. For routine atmospheric measurements, we use three broadband optical filters (F1, F2, and F3) with the following transmittance bands: 2350–5400 cm^{-1} (in combination with InSb detector), 1700–3400 cm^{-1} (in combination with InSb detector), and 650–1400 cm^{-1} (in combination with MCT detector).

The routine monitoring of FTS alignment is performed using the laboratory spectra of a HBr cell (#61) and N_2O cell (#3). Since the first HBr spectrum measurement in April 2012, we controlled the state of IFS 125HR approximately once a month. The modulation efficiency and phase error affecting the instrumental line shape were retrieved from cell spectra using LINEFIT v.14.5 software [31]. These values obtained using HBr cell during 2012–2022 are given in Figure 2a,b.

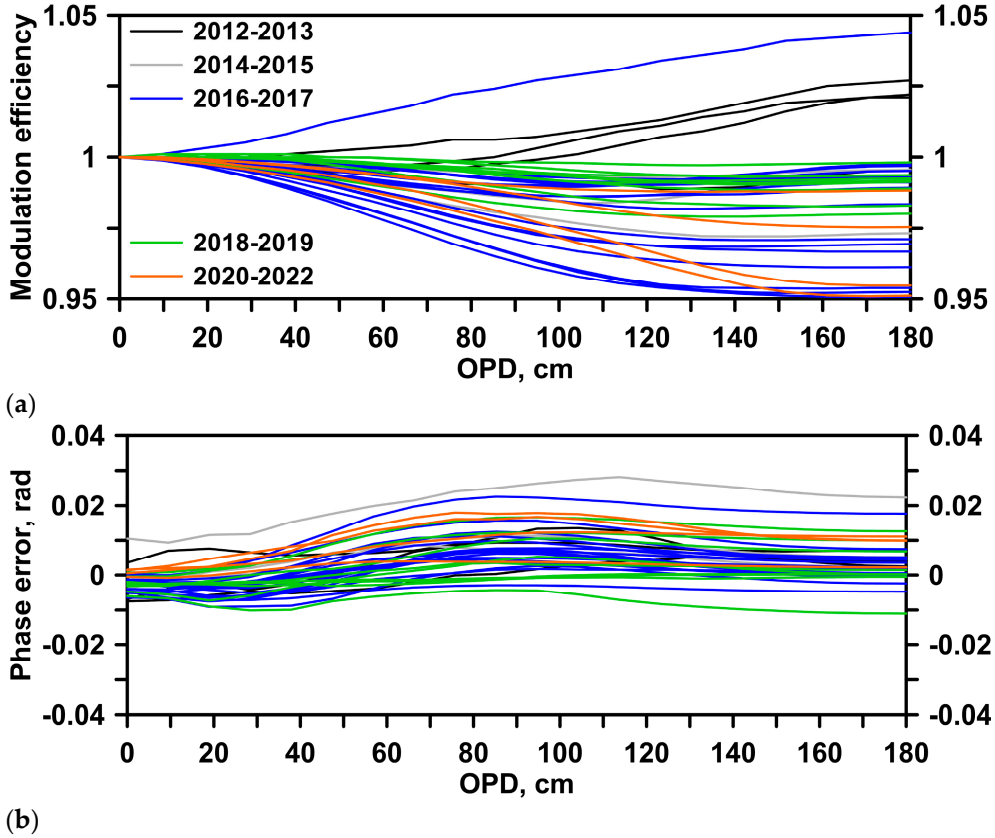

Figure 2. Modulation efficiency (**a**) and phase error (**b**) as a function of OPD for the 2012–2022.

In total, within the period of 2009–2022, FTIR observations at the St. Petersburg site have been performed for 1045 days (~19300 single spectra), i.e., ~80 days per year on average. Between 2009 and 2022, there were four gaps in the FTIR data due to FTS and solar tracker failures and their subsequent troubleshooting.

Atmospheric FTIR observations use the sun as a light source, and therefore these types of remote measurements are performed under clear sky conditions or when the cloud cover has gaps sufficient to record at least a single spectrum. The distribution of measurement days over a year is uneven for St. Petersburg, due to high cyclonic activity in autumn and winter, and also due to the significant seasonal dependence of diurnal solar illumination: from 5 h 51 min (winter solstice) to 18 h 50 min (summer solstice). On the 22nd of December the value of the SZA (sun zenith angle) is larger than 83.50° during the whole day. Diurnal, seasonal and inter-annual cumulative distributions of the number of single spectra acquired using all three optical filters (F1, F2, and F3) are given in Figure 3a, Figure 3b and Figure 3c, respectively.

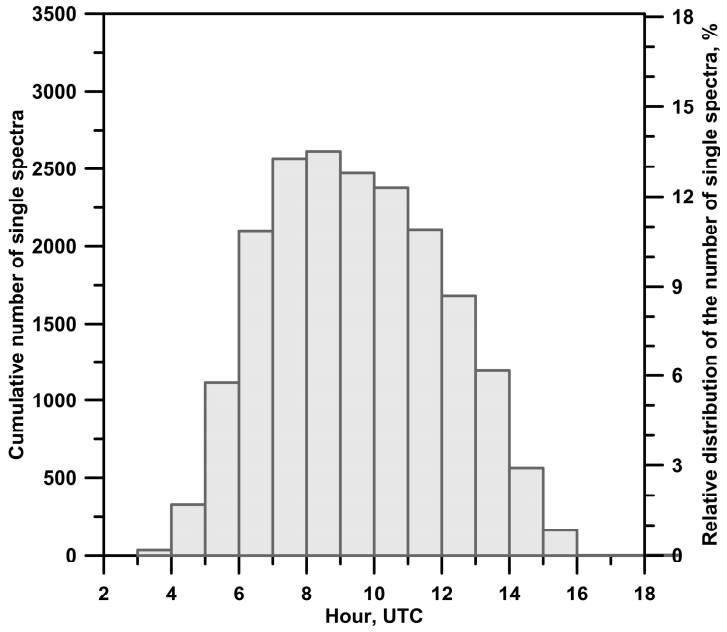

(**a**)

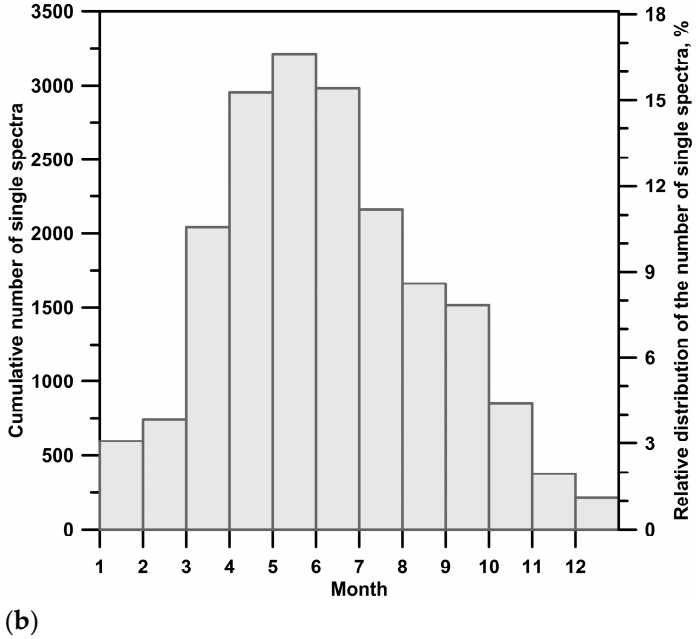

(**b**)

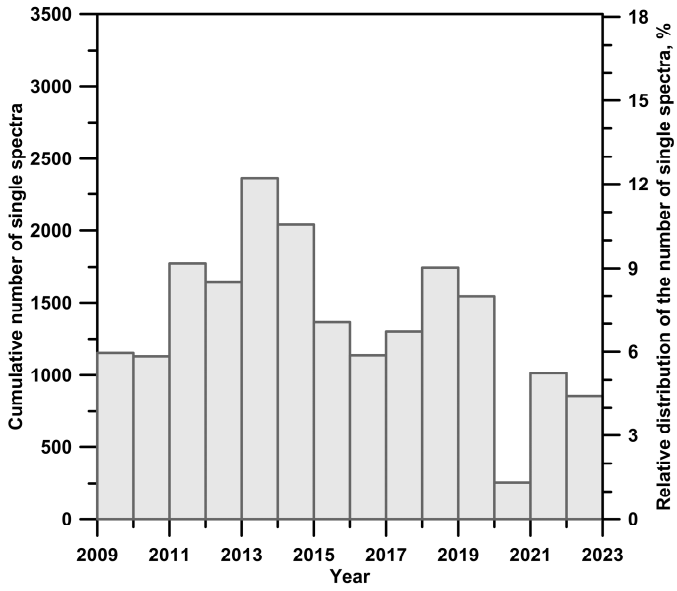

(**c**)

Figure 3. Diurnal (**a**), seasonal (**b**) and inter-annual (**c**) distribution of the cumulative number of single spectra acquired at the St. Petersburg site in 2009–2022. All plots: left *Y*-axis shows the absolute number of single spectra; right *Y*-axis shows relative value (in percent) which is equal to absolute cumulative number of single spectra normalized to the total number (~19300) of single spectra measured in 2009–2022.

The typical configuration of the FTIR system, which is used for the GHG monitoring in the MIR spectral region at the STP station, is given in Table 2. An example of solar spectra recorded at the St. Petersburg site is presented in Figure 4.

Table 2. Typical FTIR system setup for MIR atmospheric measurements of GHG at the St. Petersburg station.

Detector	**LN-Cooled InSb**
Beamsplitter	KBr
Fieldstop, mm	0.8–1.3
$\Delta\nu$, cm^{-1} (OPD, cm)	0.005 (180)
Registered spectral range, cm^{-1}	1700–3400 (optical filter F2)
Number of scans	4–10

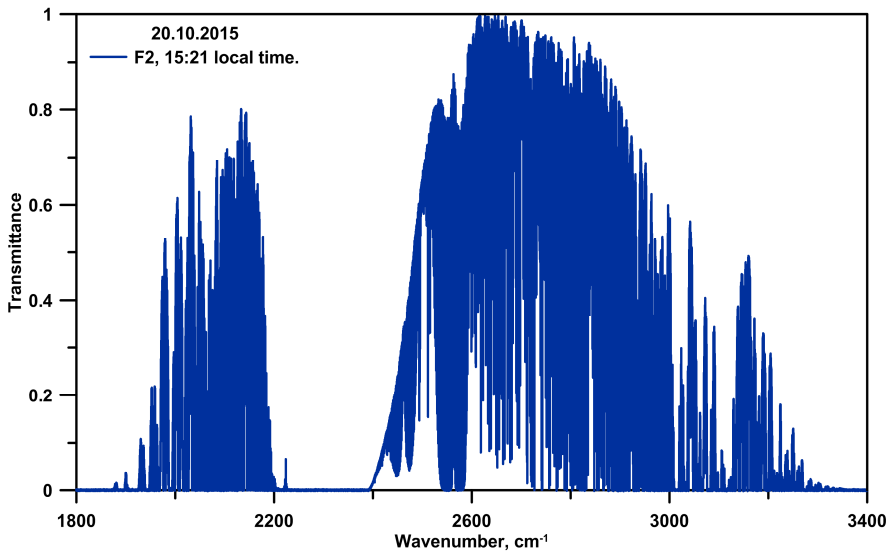

Figure 4. An example of FTIR solar spectra acquired using F2 optical filter and LN-cooled InSb detector.

2.2. Inverse Methods and Retrieval Strategies

If we consider the ground-based FTIR observations, a solution of an inverse problem implies deriving quantitative information on total columns (TCs) and/or the volume mixing ratio (VMR) vertical profiles of target gases in the atmosphere from the MIR spectra of solar radiation. From a physical point of view, the retrieval of a gas VMR profile is possible due to the dependence of the spectral line shapes of the gas molecules on the vertical profiles of temperature and pressure in the atmosphere. The formalism for solving such an ill-posed problem of atmospheric sounding, which requires a certain amount of a priori information, has been developed by Tikhonov [32] and Rodgers [33,34]. Optimal Estimation (OE) and Tikhonov–Phillips regularization (T–P) are the two most common algorithms implemented in the retrieval codes SFIT (https://wiki.ucar.edu/display/sfit4/, accessed on 23 March 2024) [35,36] and PROFFIT [37,38]. Both codes are used by IRWG NDACC groups for the FTIR spectra processing. The details on the theory of inverse techniques and practical application to the ground-based FTIR observations can be found in the papers by Tikhonov [32], Rodgers [34], Pougatchev et al. [35], Rinsland et al. [36], Hase et al.[37], Sussmann et al. [39], and García et al. [40]. T–P L1 regularization [41] is used in the TC/VMR retrievals in the cases where the covariance matrix S_a, which is a critical point for OE, cannot be constructed using reliable independent observations [42].

The TCs and VMR profiles of atmospheric CH_4, N_2O, CO, HCN, C_2H_6, HCl, HF, O_3, HNO_3, and $ClONO_2$ are routinely measured at the St. Petersburg site. Corresponding retrieval results for all these trace gases are available at the NDACC database (https://www-air.larc.nasa.gov/missions/ndacc/data.html, accessed on 23 March 2024) in the form of HDF files. In addition to the above-mentioned NDACC mandatory list of species, the following gases are measured at the STP site: CO_2, H_2O, CFC-11, CFC-12, HCFC-22, H_2CO, CH_3OH, HCOOH, C_2H_2, OCS, NH_3, NO_2 and N_2. Data on CFC-11, CFC-12, HCFC-22, H_2CO, OCS can also be found at NDACC database, and the information on other gases can be provided upon request. In the current work we are focusing on the FTIR monitoring of long-lived greenhouse gases (CH_4, N_2O, and CO_2). All the retrievals of these species have been conducted by SFIT4 tools (v. 4.09.4.4).

For the greenhouse gases from the IRWG mandatory list (i.e., CH_4, N_2O), the retrieval of TCs and VMR profiles from high resolution FTIR spectra acquired at the STP site is mainly based on the IRWG Uniform Retrieval Guidelines [43]. This document contains the recommended retrieval strategies, which can be used by most of the FTIR sites with various geographical, climate and weather conditions. For CO_2, we use retrieval strategies which were recently developed by the IRWG community (for details, please, see [44]).

The a priori information, which is homogeneous for all IRWG observational sites, was constructed for most of the trace gases using WACCM v.6 simulations (Whole Atmosphere Community Climate Model, https://ncar.ucar.edu/what-we-offer/models/whole-atmosphere-community-climate-model-waccm, accessed on 23 March 2024) [45]. It includes:

- site-specific a priori VMR profiles of the retrieved and interfering species;
- site-specific a priori covariance matrixes (S_a) for the retrieved and interfering species (constructed using WACCM v.6 data on variability of VMR profiles).

In our retrievals, all priori information is not time-dependent, i.e., we set it once and keep it unchanged when processing all the years of measurements (2009–2022), so the detected temporal variations of the target gases are completely based on observations.

A homogeneous input information on atmospheric pressure and temperature profiles, which is necessary for the forward model calculations, is provided by NOAA/NWS/National Centers for Environmental Prediction (NCEP) in the form of daily (at 12:00 UTC)

profiles of temperature and geopotential heights on 18 pressure levels from 1000 to 0.4 hPa at NDACC stations (https://www-air.larc.nasa.gov/missions/ndacc/data.html?NCE12.00UTCP=ncep-list, accessed on 23 March 2024). Spectroscopy linelists are critical input data for getting reliable retrieval results. HITRAN databases [46–49] and ATM linelists created by G. Toon [50] (NASA Jet Propulsion Laboratory, http://mark4sun.jpl.nasa.gov/toon/linelist/linelist.html, accessed on 23 March 2024) were mainly used for this purpose. For each target gas we provided information on spectroscopy linelists in the third column of Table 3. Information about solar spectral lines according to [51] is incorporated into SFIT4 processing tools.

Table 3. Overview of retrieval strategies used at the STP FTIR site. Species from the IRWG mandatory list are marked by asterisk (*). The designation "L1" in the fifth column denotes the first-order Tikhonov–Phillips constraint.

Target Gas	Spectral Intervals, cm^{-1}	Spectroscopic Linelist	Retrieved Interfering Gases	Regularization Type	References
CH_4 *	2613.70–2615.40 2835.50–2835.80 2921.00–2921.60	HITRAN 2000 (with 2001 updates)	HDO, H_2O, CO_2, NO_2	T–P L1	[39,43]
CO_2	2620.55–2621.10 2626.40–2626.85 2627.10–2627.60 2629.275–2629.950	HITRAN 2008, HITRAN 2009 for H_2O	H_2O, HDO, CH_4	T–P L1	[44]
N_2O *	2481.30–2482.60 2526.40–2528.20 2537.85–2538.80 2540.10–2540.70	HITRAN 2008	CO_2, H_2O, CH_4, O_3	T–P L1	[43]

3. Results and Discussion

3.1. Characterizing Retrieval Results: Spectral Fitting, Uncertainty Analysis and Averaging Kernels

To describe retrieval results, the following main characteristics are usually reported (the examples can be found in the papers [42,44,52–54]:

- the RMS discrepancy between the observed and simulated spectra as a measure of the quality of spectral fitting (see column 3 of Table 4). The typical examples of spectral fitting for corresponding spectral intervals used in the CH_4, CO_2, and N_2O retrievals are given in Figures 5, 6 and 7, respectively;
- the uncertainty (error) budget including the analysis of random, systematic, and smoothing uncertainties (see columns 7–9 of Table 4);
- the averaging kernels (AVKs) for VMR, the "sensitivity" of the retrievals to the measurements [55] (Figures 8–10), and the value of degrees of freedom for the signal (DOFS; see columns 5–6 of Table 4), which characterize the vertical sensitivity of the retrieval. The sensitivity at altitude level i is calculated as the sum of the elements of the corresponding averaging kernel $\Sigma_k AVK_{ik}$;
- retrieved total columns (TCs), column-averaged dry-air mole fraction (X_{GAS}) (see columns 2–3 of Table 4). We calculated X_{GAS} by dividing the total column of a target gas (TC_{GAS}) by the dry pressure column (DPC) parameter [44,56]:

$$X_{GAS} = \frac{TC_{GAS}}{DPC} \quad (1)$$

$$DPC = 0.2095\frac{P_S}{g(\varphi)m_{dryair}} - TC_{H2O}\frac{m_{H2O}}{m_{dryair}} \quad (2)$$

where m_{dryair}—the molecular mass of dry air (28.964 g mol^{-1});

m_{H2O}—molecular mass of H_2O (18.02 g mol^{-1});

P_s—surface pressure (mb), which is taken from NCEP input data used in the retrievals;

$g(\varphi)$—the latitude-dependent gravitational acceleration;

TC_{H2O}—the total column of water vapor, which is a result of separate retrieval of H_2O TC.

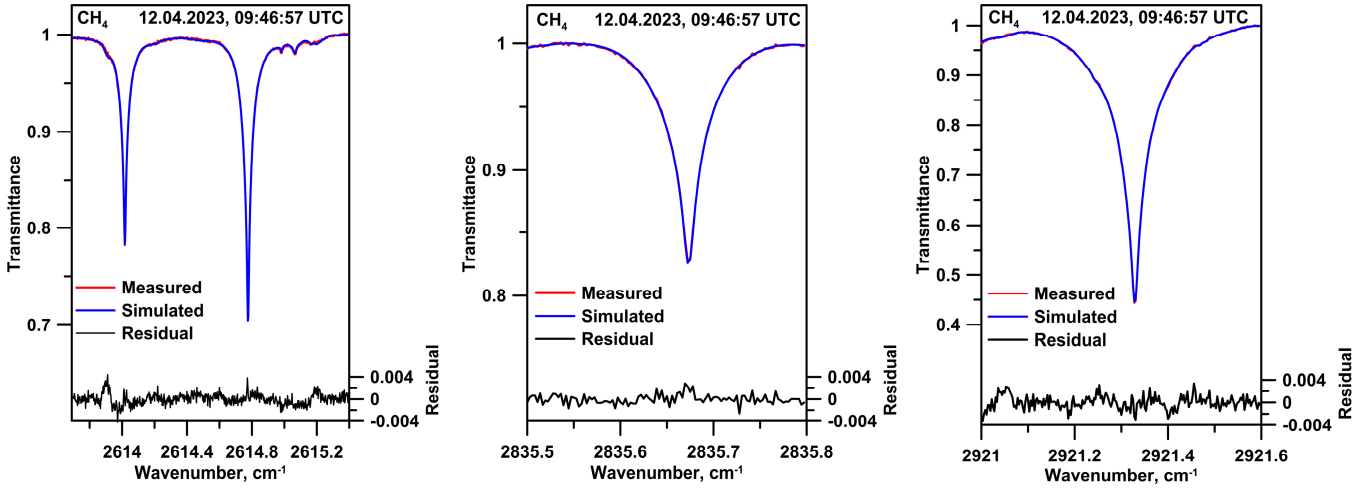

Figure 5. Spectral fitting in the spectral intervals used for the CH_4 retrievals (the spectrum was acquired 12 April 2023, 09:46:57 UTC).

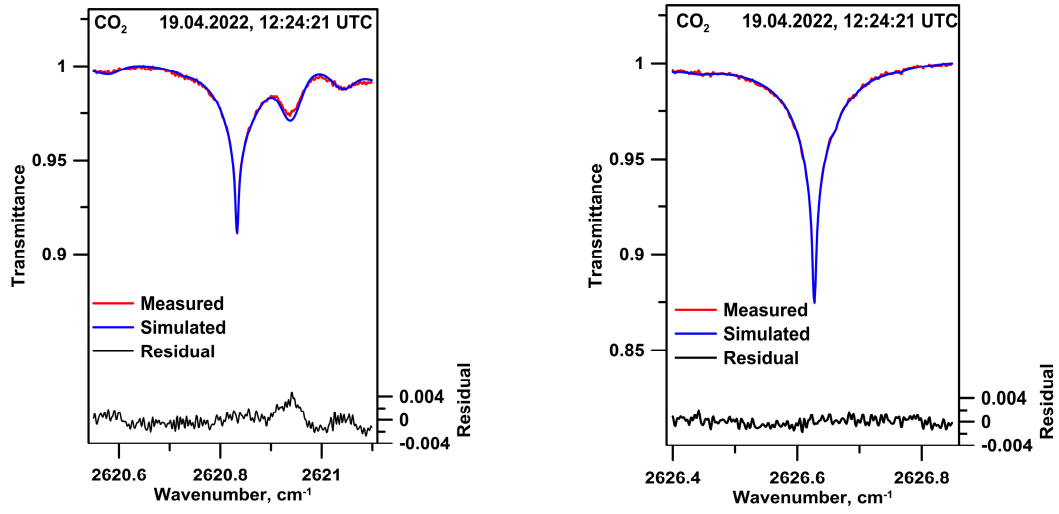

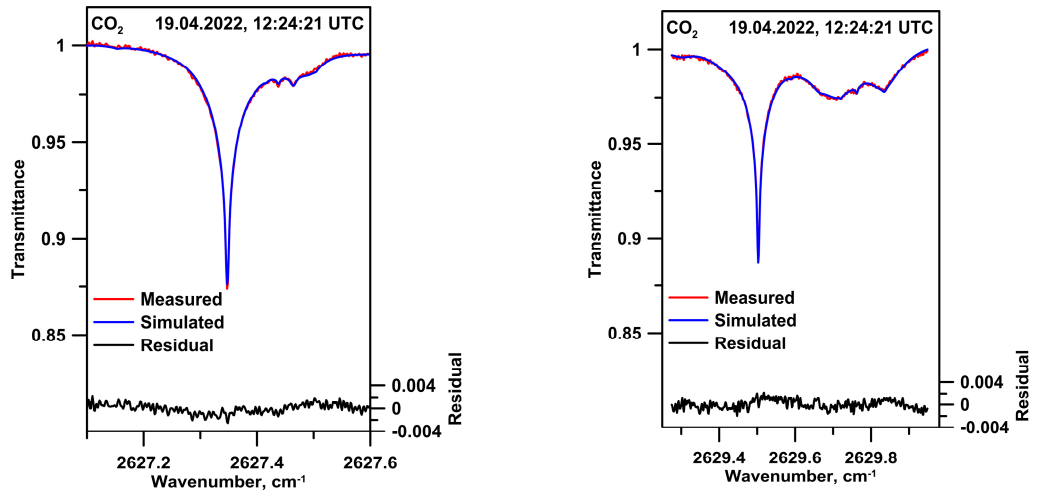

Figure 6. Spectral fitting in the spectral intervals used for the CO_2 retrievals (the spectrum was acquired 19 April 2022, 12:24:21 UTC).

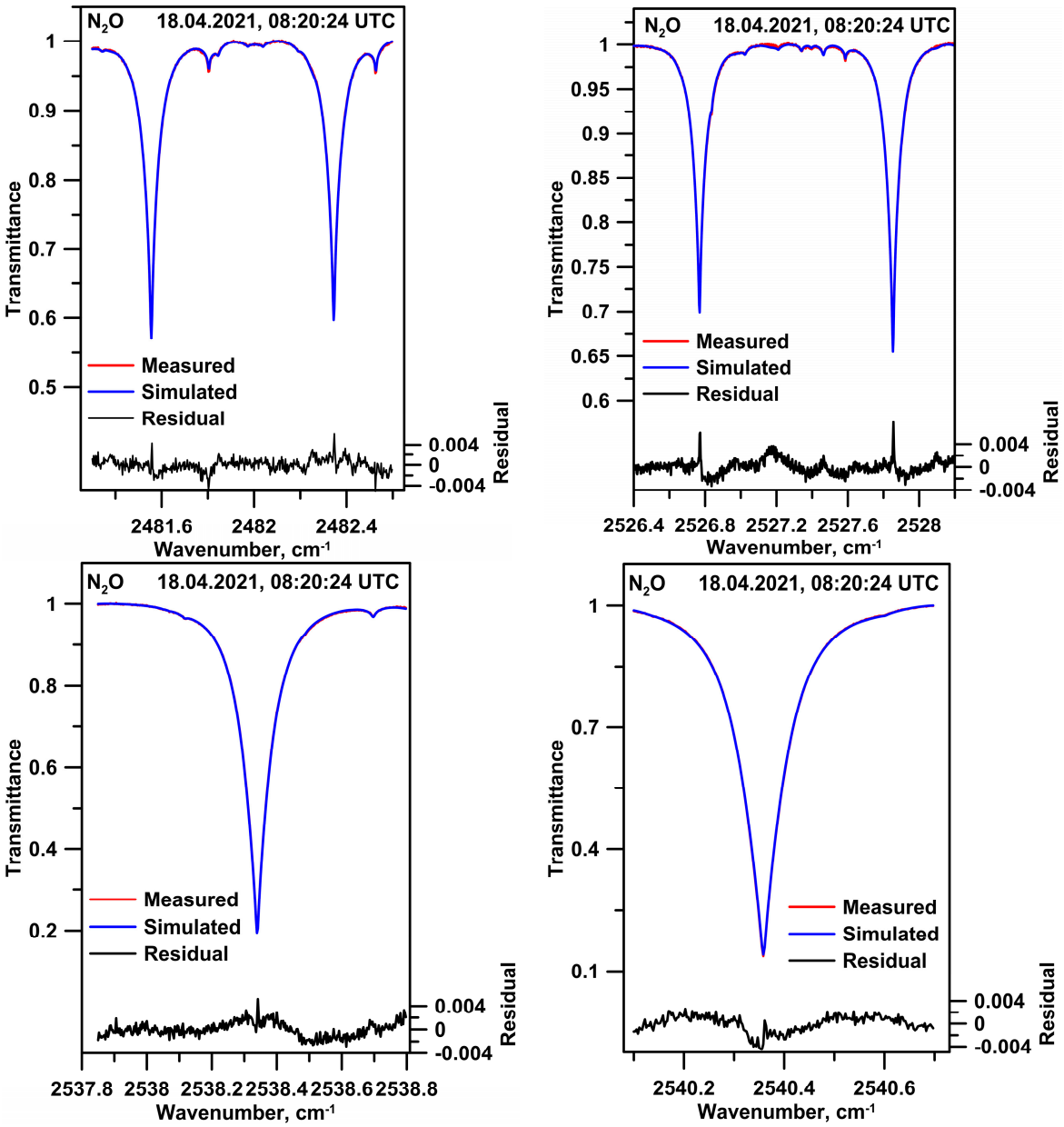

Figure 7. Spectral fitting in the spectral intervals used for the N_2O retrievals (the spectrum was acquired 18 April 2021, 08:20:24 UTC).

Table 4 contains information about the mean (M) values of TC, X_{GAS}, RMS, DOFS, systematic, random, and smoothing uncertainties averaged over the entire measurement period (2009–2022); standard deviation (σ) is given as a measure of the variability of the reported values.

The "AVK for VMR" functions and the "sensitivity for TC" functions have gas-specific altitude dependence (Figures 8–10). Together with the DOFS value (which is equal to the trace of AVK matrix), they characterize the vertical sensitivity of FTIR observations to the abundance of a target gas. AVKs characterize the degree of smoothing of the true profile in the retrieval procedure; the sensitivity at each altitude indicates the fraction which comes to the retrieval from the measurement rather than from the a priori information. The DOFS value (a number of independent pieces of information) can be interpreted in our case as a number of atmospheric layers for target gas which can be retrieved independently from observations. For DOFS, we show two values in Table 4: the value of DOFS for the entire atmospheric column and the value of DOFS which was calculated separately for the troposphere (0–10 km). So, according to Table 4, only the TC value can be obtained in the case of the CO_2 retrieval, since the corresponding DOFS < 2.0 (i.e., we have an independent piece of information on only one atmospheric layer). Columns in two atmospheric layers can be obtained in the cases of the CH_4 and N_2O retrieval: in the troposphere where DOFS > 1.0 and in the remaining overlying atmosphere (10–106 km).

The quantitative evaluation of uncertainties based on the formula developed by Rodgers [33,34] is incorporated into the SFIT4 retrieval tools. This ensures the homogeneity of error estimates obtained by different IRWG groups. The error budget for all target species is given in Table 4, and it consists of the following components:

- the systematic error which originates from the systematic uncertainties of the following forward model/input parameters: spectroscopy (line intensity, line broadening by pressure and temperature, solar line intensity), sun zenith angle (SZA), curvature of the spectrum baseline, phase, optical path difference (OPD), field of view (FOV). The systematic error budget is mainly defined by uncertainties in the spectroscopic information, i.e., line intensities and broadening factors [40];
- random error, which includes measurement error (due to measurement noise), random uncertainties of forward model/input parameters, uncertainties of the parameters of the retrieval algorithm, interference error (due to retrieved interfering gases) and smoothing error. The dominant inputs into random uncertainty are as follows: measurement noise, baseline uncertainty, and uncertainties in the input temperature profile [40,42];
- the smoothing error, which is assumed to be random in our study (with no systematic component), reflects the uncertainty due to the limited vertical resolution of the FTIR observations.

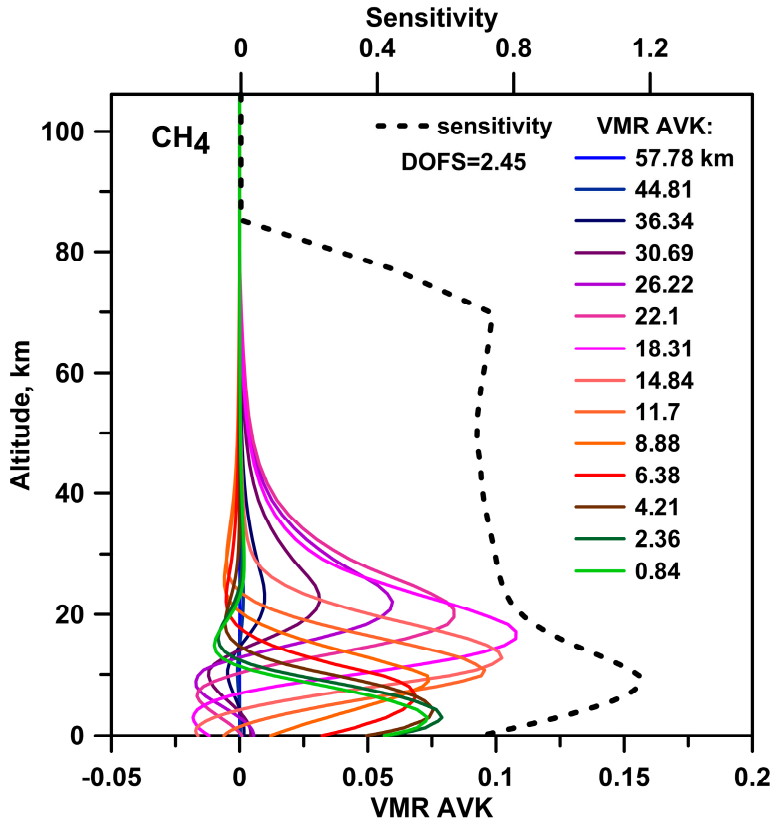

Figure 8. Typical AVKs for the CH_4 VMR retrievals (ppmv/ppmv) for a number of altitudes (solid lines, see the legend) and the sensitivity (dashed line) to the CH_4 abundance as a function of altitude (the spectrum was acquired 12 April 2023 09:46:57 UTC).

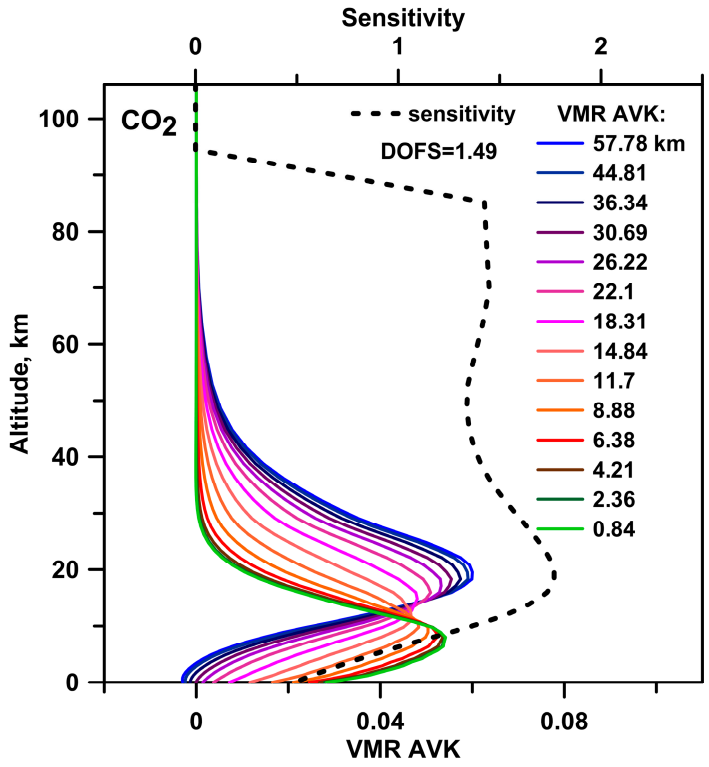

Figure 9. Typical AVKs for the CO_2 VMR retrievals (ppmv/ppmv) for a number of altitudes (solid lines, see the legend) and the sensitivity (solid line) to the CO_2 abundance as a function of altitude (the spectrum was acquired 19 April 2022 12:24:21 UTC).

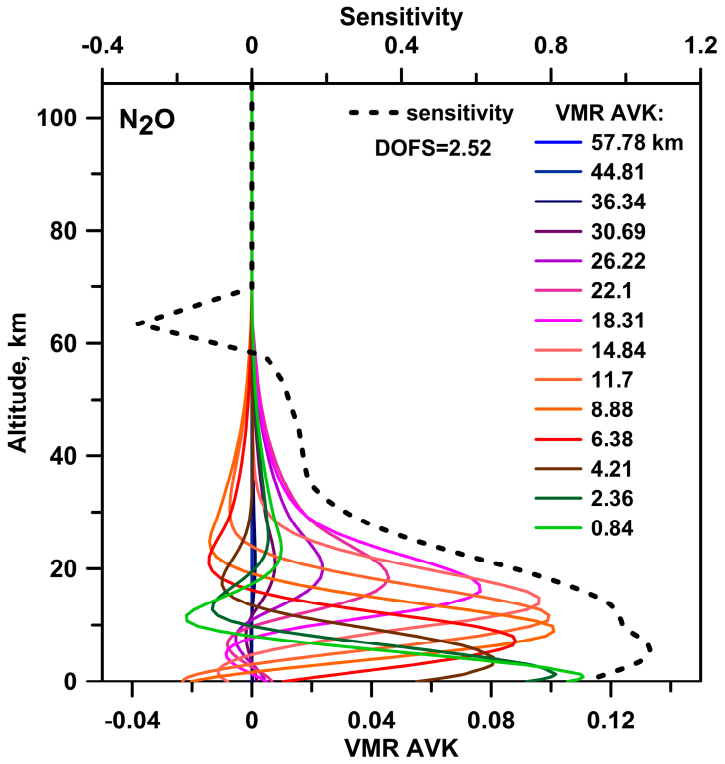

Figure 10. Typical AVKs for the N_2O VMR retrievals (ppmv/ppmv) for a number of altitudes (solid lines, see the legend) and the sensitivity (dashed line) to the N_2O abundance as a function of altitude (the spectrum was acquired 18 April 2021 08:20:24 UTC).

The average values of random and systematic uncertainties, as well as smoothing errors estimated for all three gases on the bases of the results of the fourteen-year retrievals at the STP site are of 1–2%, 3–4% and less than 0.5%, respectively (see Table 4, columns 7–9).

Table 4. Mean values (M) and standard deviations (σ) of TC, X_{GAS}, DOFS ("total"—for the entire atmospheric column, and "tropo"—for the troposphere), and also random, systematic, and smoothing uncertainties. All values were obtained as a result of FTIR spectra processing within the period 2009–2022.

Target Gas	TC, molec/cm²	X_{GAS}, ppm	RMS, %	DOFS		Random Uncertainty, %	Systematic Uncertainty, %	Smoothing Uncertainty, %
				Total	Tropo			
	M ± σ	M ± σ	M ± σ	M ± σ	M ± σ	M ± σ	M ± σ	M ± σ
CH_4	$(3.885 \pm 0.089)\cdot10^{19}$	1.807 ± 0.038	0.14 ± 0.03	2.5 ± 0.3	1.3 ± 0.2	1.5 ± 0.9	3.6 ± 0.1	0.5 ± 0.1
CO_2	$(8.79 \pm 0.23)\cdot10^{21}$	409 ± 10	0.14 ± 0.03	1.4 ± 0.2	0.7 ± 0.1	2.2 ± 0.9	3.4 ± 0.2	0.5 ± 0.4
N_2O	$(6.59 \pm 0.12)\cdot10^{18}$	0.3071 ± 0.0055	0.18 ± 0.06	2.6 ± 0.2	1.6 ± 0.1	1.2 ± 0.2	2.6 ± 0.1	0.2 ± 0.1

3.2. Time Series Analysis: Long-Term Trends of GHG TCs

Figures 11–13 display CH_4, CO_2, and N_2O TC and X_{GAS} time series for 2009–2022 as measured at the STP FTIR station. Previously, data filtering was carried out. Measurements with high RMS/DOFS values [39] which were beyond the average value of RMS/DOFS plus 3σ were rejected. In addition to the RMS/DOFS criterion, the outliers that manifested in obviously inadequate (extremely low or extremely high beyond the 3σ variability limits) values of the LLGHG TCs were also excluded from the time series. Before filtering, the LLGHG time series included 6278 single measurements each. After applying

the above mentioned criteria, the number of single measurements for CH_4, CO_2 and N_2O became 6168, 6103 and 6163, respectively.

We assumed that the analyzed time series of *TC* can be approximated by a model function $F_{TC}(t)$ that is the sum of a linear function and a set of *N* harmonic functions:

$$F_{TC}(t) = a + b\bar{t} + \sum_{i=1}^{N} c_i \cos(\alpha_i t + \varphi_i) \quad (3)$$

where *t* is time; and *a*, *b*, c_i, α_i and φ_i are the coefficients to be determined.

This is a typical approach which is widely used for the analysis of time series of atmospheric trace gases [54]. The TC long-term trend is equal to the coefficient *b*, which determines the slope of the linear function (see Equation (3)). To obtain statistical characteristics (the mean value of *b*, the confidence intervals/uncertainty of *b*) of long-term trends for CH_4, CO_2 and N_2O, the analysis of TC time series of target gases was carried out in the following three steps:

1. Harmonic analysis of the time series of LLGHG TCs. For this purpose, time series were previously detrended using the simple linear regression. After detrending, the Lomb–Scargle method, which is a modification of Fourier analysis for uneven time series, was applied [57–59]. The outcome is a set of *n* periods/frequencies having peaks (maxima) of spectral density in periodogram.
2. Estimation of an optimal set of *N* harmonic functions (from the whole set *n*) which provides the best approximation. To achieve this goal, we evaluated the performance of a model $F_{TC}(t)$ on unseen data (cross-validation technique). It involves dividing the available time series (TC) into multiple subsets, using one of these subsets as a validation set, and training the model on the remaining subsets (https://www.geeksforgeeks.org/cross-validation-machine-learning/, accessed on 23 March 2024). We made this analysis multiple times, including *i* most significant harmonic functions at each step (starting from $i = 1$ and ending with $i = n$). For each step we determined the RMS value of the discrepancy between validation set and model function $F_{TC}(t)$. The optimal number *N* provides the minimum value of the RMS discrepancy between the model and the validation set. Approximations $F_{TC}(t)$ for 2009–2022, which were constructed with the optimal numbers *N*, are presented in Figures 11–13 by solid lines.
3. Evaluation of the mean value of a trend (coefficient *b*) and its confidence intervals/uncertainty. For this purpose, the bootstrapping approach was implemented [54,60]. To characterize the distribution function for trend (allowing us to estimate the mean slope *b* and 1σ uncertainty as distribution halfwidth), we used a bootstrap population of ~400 (a further increase of this number does not lead to any noticeable changes in the results).

At all stages, data fitting was performed by the least squares method. The X_{GAS} trends were determined in the same three-step way as for TC.

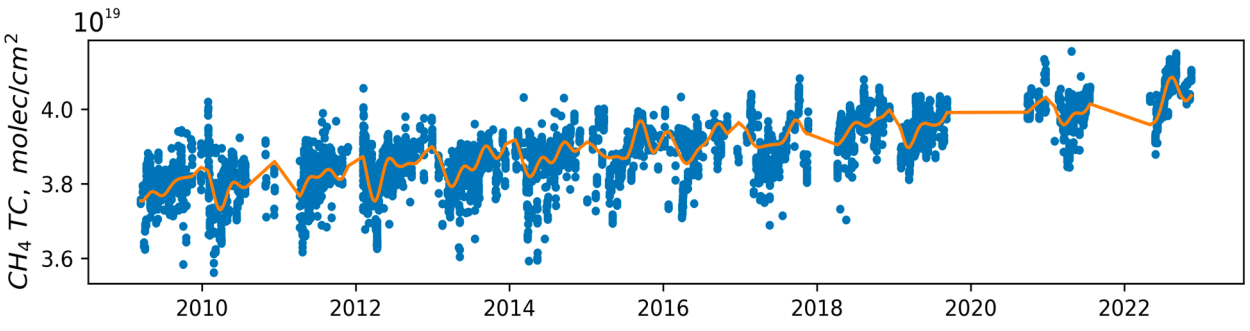

(**a**)

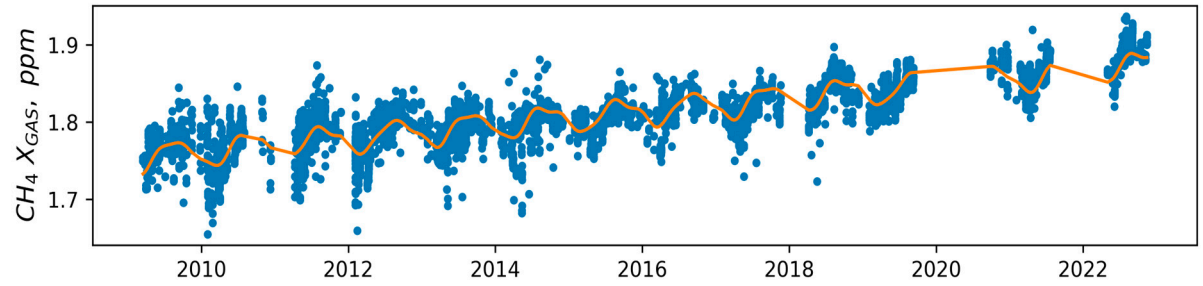

(**b**)

Figure 11. (**a**) The CH_4 TC time series (blue dots) and its approximation (orange line); (**b**) the CH_4 X_{GAS} time series (blue dots) and its approximation (orange line).

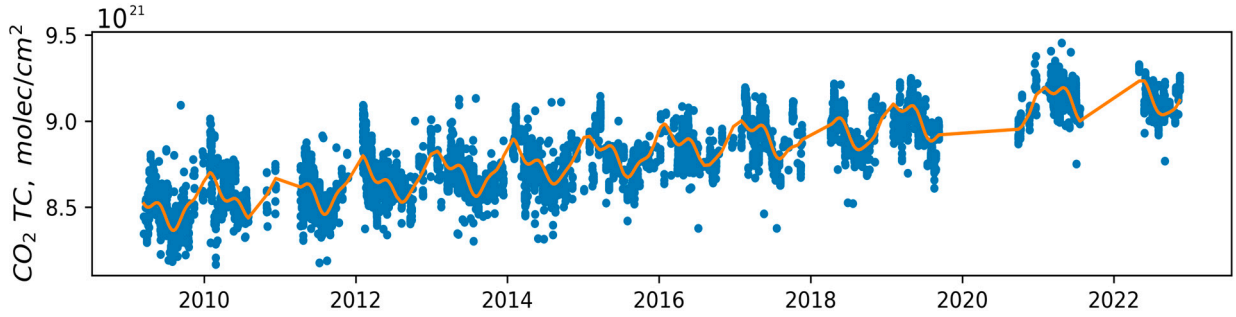

(**a**)

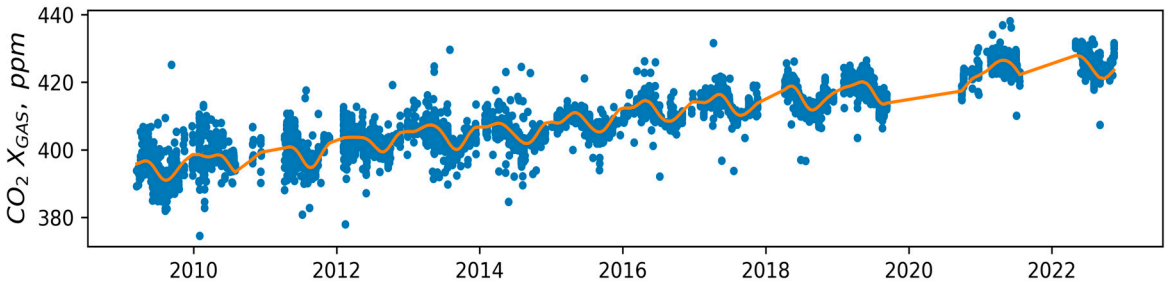

(**b**)

Figure 12. (**a**) The CO_2 TC time series (blue dots) and its approximation (orange line); (**b**) the CO_2 X_{GAS} time series (blue dots) and its approximation (orange line).

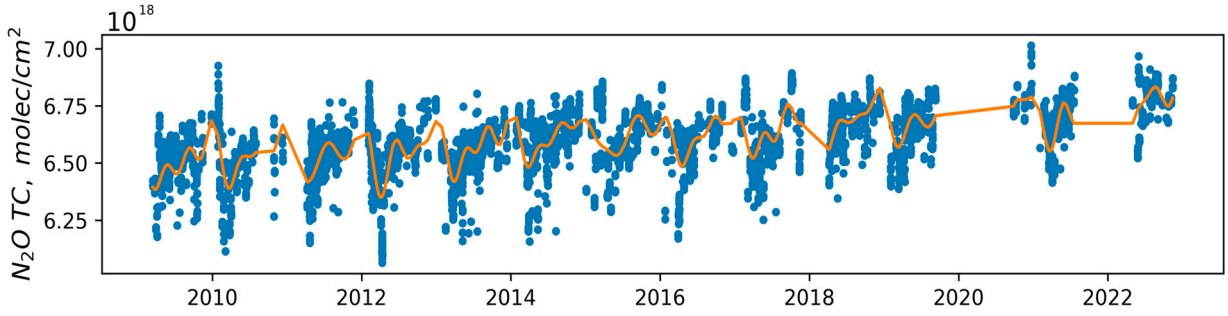

(**a**)

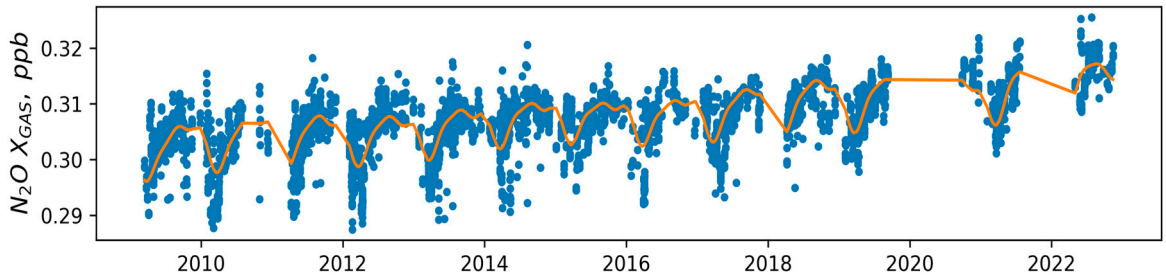

(**b**)

Figure 13. (**a**) The N_2O TC time series (blue dots) and its approximation (orange line); (**b**) the N_2O X_{GAS} time series (blue dots) and its approximation (orange line).

Table 5 presents the estimates of the coefficient *b* (slope) which characterize the long-term trends of LLGHGs' TCs and X_{GAS} in the atmosphere for different periods of time. The second column of this table shows the mean values of the long-term trends of target gases with 95% confidence intervals (2σ) for the fourteen-year (2009–2022) period of FTIR measurements at the STP station observations. The third column (with subcolumns) presents the results for the eleven-year (2009–2019) observations. If the variability of TC is influenced by atmospheric pressure at the observational site, then the transition from the TC to the X_{GAS} excludes the influence of atmospheric pressure variations (see Equation (2)). X_{GAS} is a value widely used in studies of the atmospheric gaseous composition; however, in our opinion, the long-term processes affecting the GHGs content in the atmospheric column can be better characterized by the TC trend rather than the X_{GAS} trend. If we take into account possible (hypothetic) trends in atmospheric pressure, we can conclude that the TC trend characterizes an increase of the total number of molecules absorbing IR radiation in the column of the atmosphere.

Reasonable agreement of CH_4 and N_2O TC trends for 2009–2019 captured by FTIR measurements at the STP site of SPbU, Izaña Observatory (IO, 28.3°N, 16.5°W, ~2370 m a.s.l.) [40], and the University of Toronto Atmospheric Observatory (TAO, 43.66°N, 79.40°W, 174 m a.s.l.) [61] can be seen if we compare the third, the fourth, and the fifth columns of Table 5. Here we should note that STP, IO and TAO are members of the NDACC network; therefore, FTIR observations and their processing are consistent in general for all three sites.

The above-described data analysis algorithm was also applied to the TC time series of CH_4, CO_2, and N_2O simulated by the ECHAM/MESSy Atmospheric Chemistry (EMAC) model (2009–2019). The EMAC model is a numerical chemistry and climate simulation system which includes sub-models describing the processes in the troposphere and in the middle atmosphere and their interaction with oceans, land and anthropogenic impacts [62,63]. The simulation includes a comprehensive atmospheric chemistry setup for the troposphere, the stratosphere and the lower mesosphere. The EMAC model profiles of trace gas concentrations, pressure and temperature were simulated directly for the geographical location of the STP site. For an accurate comparison of the model (EMAC) and the experimental (FTIR) trends, an EMAC simulation of the FTIR time series (EMAC TC_{FTIR_AVK}) was created. For this purpose, we generated a set of model profiles for the dates coinciding with the dates of FTIR measurements, after that, following the Rodgers and Connor [64] formula (see Equation (4)), model profiles were convolved (smoothed) with the AVKs of corresponding FTIR measurements as follows:

$$x_s = \boldsymbol{A}(x - x_a) + x_a \quad (4)$$

where x is the EMAC profile of a target gas; x_s is the smoothed EMAC profile of a target gas; $\boldsymbol{A}$ is the FTIR AVK matrix; x_a is the FTIR a priori profile of target gas.

Finally, smoothed EMAC profiles (x_s) were used for the calculation of total columns (EMAC TC_{FTIR_AVK}). Trend estimations for EMAC TC_{FTIR_AVK} of LLGHGs are given in the

sixth column of Table 5. It can be seen that the trends of TC obtained from the FTIR monitoring results and from model simulations for N_2O and CO_2 agree within 3σ. The largest difference in the TC trends, amounting to 0.28% yr^{-1} and exceeding the 3σ limit, was obtained for CH_4.

Table 5. The LLGHGs linear trends (±2σ) in the atmosphere revealed from the results of FTIR measurements at the STP site in comparison to IO [40] and TAO [61] trends, EMAC model trends, global VMR trends obtained at the GAW in situ observational network for GHGs (WMO, 2022), and VMR trends determined using in situ observations of CH_4 and CO_2 at STP site [65]. The periods for which LLGHGs trends were estimated are given in the second row of the table.

Target Gas	Mean Trend								
	2009–2022	2009–2019				2012–2021		2013–2019	
	FTIR TC, FTIR X_{GAS}	FTIR TC	FTIR TC (IO)	FTIR TC (TAO)	EMAC $TC_{F\text{-}TIR\_AVK}$	FTIR X_{GAS}	Global In Situ VMR (GAW)	FTIR X_{GAS}	In Situ VMR
CH_4, % yr^{-1} ppb yr^{-1}	0.46 ± 0.02 8.8 ± 0.4	0.44 ± 0.04	0.43 ± 0.03	0.41 ± 0.03	0.16 ± 0.04	0.47 ± 0.05 8.5 ± 1.0	0.51 9.2	0.52 ± 0.04 9.4 ± 0.7	0.49 8.6 ± 0.8
CO_2, % yr^{-1} ppm yr^{-1}	0.56 ± 0.01, 2.28 ± 0.05	0.58 ± 0.02	-	-	0.52 ± 0.02	0.61 ± 0.02 2.52 ± 0.07	0.61 2.46	0.61 ± 0.04 2.5 ± 0.1	0.60 2.42 ± 0.1
N_2O, % yr^{-1} ppb yr^{-1}	0.28 ± 0.01 0.82 ± 0.03	0.26 ± 0.02	0.31 ± 0.03	-	0.20 ± 0.02	0.30 ± 0.03 0.91 ± 0.08	0.31 1.01	0.26 ± 0.04 0.8 ± 0.1	-

The X_{GAS} trends for 2012–2021 estimated using FTIR measurements at the STP station and global VMR trends obtained at the GAW in situ observational network for GHGs [1] are presented in the seventh and eighth columns of Table 5. The ninth and tenth columns show the trends obtained using FTIR X_{GAS} data and the results of in situ monitoring of CO_2 and CH_4 VMR at the STP station in 2013–2019, respectively. It should be noted that the publication by Foka et al.[65] is devoted to the analysis of trends of in situ VMR measurements carried out at the same location where the FTIR observations were performed. A reasonable agreement (within 2σ) of the FTIR X_{GAS} trends with the in situ VMR trends reported in both papers [1,65] was obtained. When comparing trends of X_{GAS} with the results of the in situ monitoring of VMRs, it should be taken into account that, in contrast to the in situ measurements which characterize the lowest tropospheric layer (the surface layer), FTIR measurements characterize processes throughout the atmosphere with the maximum sensitivity corresponding to the middle and upper troposphere (see Figures 8–10).

We would like to draw attention to the CO_2 TC trend over the fourteen-year period 2009–2022, which is equal to 0.56% yr^{-1}. This is the lowest trend value among the CO_2 TC trends reported in Table 5 for other shorter periods: 0.58% yr^{-1} for 2009–2019; 0.61% yr^{-1} for 2012–2021 and for 2013–2019. Our analysis has shown that the reason for this result was a significant drop in the growth rate of CO_2 in 2022, which was manifested not only in the CO_2 TC data obtained at the STP site, but also in the results of the in situ measurements. For example, at the high-altitude Mauna Loa observatory (~3400 m a.s.l.) where the VMR observations are representative for the free troposphere, the CO_2 annual mean growth rate in 2021 was (2.37 ± 0.11) ppm yr^{-1}, while in 2022 it dropped to (1.81 ± 0.11) ppm yr^{-1} (the lowest value since 2008) [10,11].

It should be noted here that most NOAA GML stations are also part of the GAW WMO network. NOAA GML is the GAW WMO Central Calibration Laboratory (https://gml.noaa.gov/ccl/scales.html, accessed on 23 March 2024), responsible for maintaining and distributing the WMO Mole Fraction scale for GHGs concentrations in atmospheric air. It provides the compatibility of GHGs measurements on a global scale and

ensures the consistency of the trends obtained using GAW WMO observations (given in Table 5) with the corresponding trends according to NOAA GML data, which we discuss below. A graphical comparison of the CH_4, CO_2 and N_2O X_{GAS} trends registered at the STP site over 2009–2022, with the global growth rates of VMR obtained for the same period by the NOAA Global Monitoring Laboratory (NOAA GML [10,66]), is shown in Figure 14a–c, respectively. This figure clearly demonstrates that for CH_4 and CO_2, the fourteen-year X_{GAS} trends (solid dark blue lines) lie within the 95% confidence limits (blue stripes in Figure 14a,b) of the mean global VMR growth rates (dashed light blue lines) obtained as a result of VMR in situ measurements carried out in 2009–2022 by the NOAA GML. In contrast to CH_4 and CO_2, the N_2O X_{GAS} trend lies inside the 99% confidence interval but outside the 95% confidence interval (blue shaded area in Figure 14c) of the mean global growth rates of the N_2O VMR.

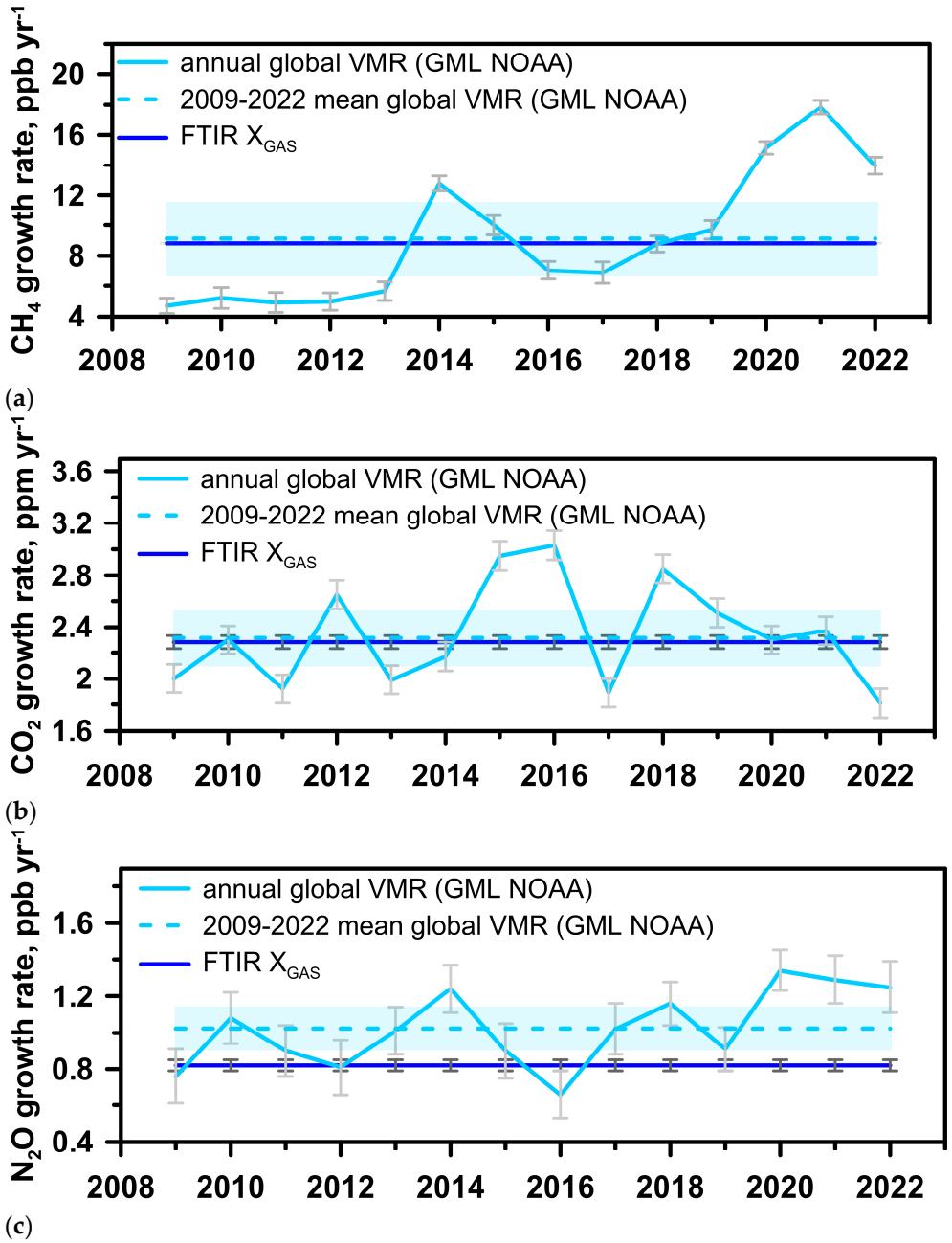

Figure 14. The CH_4 (**a**), CO_2 (**b**) and N_2O (**c**) X_{GAS} trends (solid dark blue lines) registered at the STP site (2009–2022) in comparison to the annual global growth rates of VMR (solid light blue lines) and mean global VMR growth rates (dashed light blue lines) over 2009–2022 obtained by the NOAA

Global Monitoring Laboratory [10,11,66]. Error bars are the 95% confidence intervals for X_{GAS} trends and for annual global growth rates of VMR. Blue shaded area is the 95% confidence interval for the mean global VMR growth rates over 2009–2022.

4. Summary and Conclusions

In this paper, we provide a rigorous assessment of the trend parameters of the total columns of key atmospheric greenhouse gases derived from multi-year observations at our FTIR station. Over many years, we made extensive measurements of the CO_2, CH_4, and N_2O total columns using a high resolution FTS Bruker IFS 125HR at a midlatitude station located on the Baltic Sea coast.

We applied an original approach for the TC time series analysis, which combines the Lomb–Scargle method with the cross-validation and bootstrapping techniques. As a result, the fourteen-year trends of the CO_2, CH_4, and N_2O total columns for our FTIR site were evaluated. We carried out a comparison of our results with the trends obtained by the numerical modeling, and also by the in situ and FTIR atmospheric monitoring performed at different geographical locations.

The main findings of the paper are as follows:

1. The retrieval strategies from IRWG NDACC for deriving the CO_2, CH_4 and N_2O total columns in the atmosphere from high-resolution FTIR spectra of direct solar radiation [39,43,44] have been adapted to the observational conditions at the STP station. The application of these adapted strategies resulted in the LLGHG TC retrievals with random and systematic uncertainties, on average, equal to 2.2% and 3.4% for CO_2, 1.5% and 3.6% for CH_4, 1.2% and 2.6% for N_2O, respectively. The average values of the smoothing uncertainty are of 0.5%, 0.5%, and 0.2% for CO_2, CH_4, and N_2O, respectively.
2. The average values of the CO_2, CH_4, and N_2O TCs for 2009–2022 observed at the STP site constitute $8.79 \cdot 10^{21}$ molec/cm^2, $3.885 \cdot 10^{19}$ molec/cm^2 and $6.59 \cdot 10^{18}$ molec/cm^2, respectively. The average values of X_{GAS} are equal to ~409 ppm for CO_2, ~1.807 ppm for CH_4, and ~0.3071 ppm for N_2O.
3. An evaluation of the TC and X_{GAS} trends for LLGHGs was carried out using the combined approach for time series analysis. This approach included the Lomb–Scargle method for harmonic analysis, the least squares method for data fitting, the cross-validation algorithm to determine the optimal number of harmonic functions, and the bootstrapping technique to estimate the confidence intervals of trends. The fourteen-year (2009–2022) trends of TCs and X_{GAS} estimated using such a combined approach are as follows: (0.56 ± 0.01) % yr^{-1} and (2.28 ± 0.05) ppm yr^{-1} for CO_2; (0.46 ± 0.02) % yr^{-1} and (8.8 ± 0.4) ppb yr^{-1} for CH_4; (0.28 ± 0.01) % yr^{-1} and (0.82 ± 0.03) ppb yr^{-1} for N_2O;
4. The TCs and X_{GAS} trends of LLGHGs observed at the STP site are in general agreement with the results of in situ VMR monitoring carried out at the same geographical location in the period 2013–2019 (Foka et al., in print), and with the independent estimates of global VMR growth rates obtained by the GAW network in the period 2012–2021 (WMO, 2022) and the NOAA Global Monitoring Laboratory in the period 2009–2022 [10,11,66]. There is reasonable agreement between the CH_4 and N_2O TC trends for 2009–2019 at the STP site, at Izaña Observatory [40], and also at the University of Toronto Atmospheric Observatory [61].
5. A comparison of the EMAC model results with the FTIR data shows that for N_2O and CO_2, the EMAC and FTIR trends of TC agree within 3σ. The largest difference in the experimental and model TC trends, amounting to 0.28% yr^{-1} and exceeding the 3σ limit, was obtained for CH_4.

Author Contributions: Conceptualization: M.M.; Methodology: M.M.; Formal analysis and investigation: M.M. and B.M.; Writing—original draft preparation: M.M.; Writing—review and editing: D.I., V.K., A.P. (Anatoly Poberovskii), A.P. (Alexander Polyakov), K.H.I., B.M., S.F. and E.A.;

Funding acquisition: E.A.; Resources: A.P. (Anatoly Poberovskii), A.P. (Alexander Polyakov), K.H.I., B.M., D.I., V.K. and S.F.; Supervision: M.M. All authors have read and agreed to the published version of the manuscript.

Funding: The authors acknowledge Saint-Petersburg State University for a research project 123042000071-8 (GZ_MDF_2023-2, PURE ID 93882802). N_2O data analysis and trend estimation were carried out in the frame of this Project.

Data Availability Statement: FTIR data on CH_4 and N_2O TCs are available at the NDACC database (https://www-air.larc.nasa.gov/missions/ndacc/data.html, accessed on 1 March 2024) in the form of HDF files. FTIR data on CO_2 TCs can be provided upon request (please, contact Maria Makarova m.makarova@spbu.ru).

Acknowledgments: The authors gratefully thank James Hannigan, Emmanuel Mahieu, Thomas Blumenstock, Frank Hase, Corinne Vigouroux and Bavo Langerock for their assistance in FTIR retrievals. The authors thank Oliver Kirner for providing the EMAC model data in the frame of our cooperation in the period between 2016 and 2021. The authors thank the Resource Center "Geomodel" of the SPbU Research Park for providing observational facilities (FTIR spectrometer Bruker IFS 125HR).

Conflicts of Interest: The authors declare that they have no conflicts of interest.

References

1. WMO Greenhouse Gas Bulletin, No. 18, 26 October 2022, ISSN 2078-0796. Available online: https://library.wmo.int/idurl/4/58743 (accessed on 23 March 2024).
2. Montzka, S.A. The NOAA Annual Greenhouse Gas Index (AGGI). National Oceanic and Atmospheric Administration (NOAA) Earth System Research Laboratories Global Monitoring Laboratory. 2022. Available online: http://www.esrl.noaa.gov/gmd/aggi/aggi.html (accessed on 23 March 202).
3. IPCC. *Climate Change 2021: The Physical Science Basis. Contribution of Working Group I to the Sixth Assessment Report of the Intergovernmental Panel on Climate Change*; Masson-Delmotte, V., Zhai, P., Pirani, A., Connors, S.L., Péan, C., Berger, S., Caud, N., Chen, Y., Goldfarb, L., Gomis, M.I., et al., Eds.; Cambridge University Press: Cambridge, UK; New York, NY, USA, 2021; 2391p.
4. Dlugokencky, E.J.; Houweling, S.; Bruhwiler, L.; Masarie, K.A.; Lang, P.M.; Miller, J.B.; Tans, P.P. Atmospheric methane levels off: Temporary pause or a new steady-state. *Geophys. Res. Lett.* **2003**, *30*, 1992. https://doi.org/10.1029/2003GL018126.
5. Kirschke, S.; Bousquet, P.; Ciais, P.; Saunois, M.; Canadell, J.G.; Dlugokencky, E.J.; Bergamaschi, P.; Bergmann, D.; Blake, D.R.; Bruhwiler, L.; et al. Three decades of global methane sources and sinks. *Nat. Geosci.* **2013**, *6*, 813–823. https://doi.org/10.1038/ngeo1955.
6. Prather, M.J.; Hsu, J.; DeLuca, N.M.; Jackman, C.H.; Oman, L.D.; Douglass, A.R.; Fleming, E.L.; Strahan, S.E.; Steenrod, S.D.; Søvde, O.A.; et al. Measuring and modeling the lifetime of nitrous oxide including its variability. *J. Geophys. Res. Atmos.* **2015**, *120*, 5693–5705. https://doi.org/10.1002/2015JD023267.
7. Patra, P.K.; Crisp, D.; Kaiser, J.W.; Wunch, D.; Saeki, T.; Ichii, K.; Sekiya, T.; Wennberg, P.O.; Feist, D.G.; Pollard, D.F.; et al. The Orbiting Carbon Observatory (OCO-2) tracks 2–3 peta-gram increase in carbon release to the atmosphere during the 2014–2016 El Niño. *Nat. Sci. Rep.* **2017**, *7*, 13567. https://doi.org/10.1038/s41598-017-13459-0.
8. Schaefer, H. On the causes and consequences of recent trends in atmospheric methane. *Curr. Clim. Chang. Rep.* **2019**, *5*, 259–274. https://doi.org/10.1007/s40641-019-00140-z.
9. WMO Greenhouse Gas Bulletin, No. 17, 25 October 2021, ISSN 2078-0796. Available online: https://library.wmo.int/idurl/4/58705 (accessed on 23 March 2024).
10. Tans, P. NOAA/GML. Available online: https://gml.noaa.gov/ccgg/trends/ (accessed on 19 October 2023).
11. Keeling, R. Scripps Institution of Oceanography. Available online: https://scrippsco2.ucsd.edu/ (accessed on 19 October 2023).
12. Liang, A.; Gong, W.; Han, G.; Xiang, C. Comparison of Satellite-Observed XCO_2 from GOSAT, OCO-2, and Ground-Based TCCON. *Remote Sens.* **2017**, *9*, 1033. https://doi.org/10.3390/rs9101033.
13. Siddans, R.; Knappett, D.; Kerridge, B.; Waterfall, A.; Hurley, J.; Latter, B.; Boesch, H.; Parker, R. Global height-resolved methane retrievals from the Infrared Atmospheric Sounding Interferometer (IASI) on MetOp. *Atmos. Meas. Tech.* **2017**, *10*, 4135–4164. https://doi.org/10.5194/amt-10-4135-2017.
14. Alberti, C.; Tu, Q.; Hase, F.; Makarova, M.V.; Gribanov, K.; Foka, S.C.; Zakharov, V.; Blumenstock, T.; Buchwitz, M.; Diekmann, C.; et al. Investigation of spaceborne trace gas products over St Petersburg and Yekaterinburg, Russia, by using COllaborative Column Carbon Observing Network (COCCON) observations. *Atmos. Meas. Tech.* **2022**, *15*, 2199–2229. https://doi.org/10.5194/amt-15-2199-2022.
15. Sha, M.K.; Langerock, B.; Blavier, J.-F.L.; Blumenstock, T.; Borsdorff, T.; Buschmann, M.; Dehn, A.; De Mazière, M.; Deutscher, N.M.; Feist, D.G.; et al. Validation of methane and carbon monoxide from Sentinel-5 Precursor using TCCON and NDACC-IRWG stations. *Atmos. Meas. Tech.* **2021**, *14*, 6249–6304. https://doi.org/10.5194/amt-14-6249-2021.

16. EPA. Understanding Global Warming Potentials. Available online: https://www.epa.gov/ghgemissions/understanding-global-warming-potentials (accessed on 11 September 2023).
17. EPA. Overview of Greenhouse Gases. Available online: https://www.epa.gov/ghgemissions/overview-greenhouse-gases#CO2-references (accessed on 11 September 2023).
18. COPERNICUS. Greenhouse Gases. Available online: https://climate.copernicus.eu/climate-indicators/greenhouse-gases (accessed on 11 September 2023).
19. Andrews, J.E.; Brimblecombe, P.; Jickells, T.D.; Liss, P.S.; Reid, B. *An Introduction to Environmental Chemistry*; Blackwell Science: London, UK, 1996.
20. De Mazière, M.; Thompson, A.M.; Kurylo, M.J.; Wild, J.D.; Bernhard, G.; Blumenstock, T.; Braathen, G.O.; Hannigan, J.W.; Lambert, J.C.; Leblanc, T.; et al. The Network for the Detection of Atmospheric Composition Change (NDACC): History, status and perspectives. *Atmos. Chem. Phys.* **2018**, *18*, 4935–4964. https://doi.org/10.5194/acp-18-4935-2018.
21. Lutsch, E.; Strong, K.; Jones DB, A.; Blumenstock, T.; Conway, S.; Fisher, J.A.; Hannigan, J.W.; Hase, F.; Kasai, Y.; Mahieu, E.; et al. Detection and attribution of wildfire pollution in the Arctic and northern midlatitudes using a network of Fourier-transform infrared spectrometers and GEOS-Chem. *Atmos. Chem. Phys.* **2020**, *20*, 12813–12851. https://doi.org/10.5194/acp-20-12813-2020.
22. Ionov, D.V.; Poberovskii, A.V.; Ionov, V.V. Spectroscopic Remote Sensing of NO_2 Levels in Urban Air. *J. Appl. Spectrosc.* **2017**, *84*, 109–113. https://doi.org/10.1007/s10812-017-0435-1.
23. Foka, S.C.; Makarova, M.V.; Poberovskii, A.V.; Timofeev, Y.M. Temporal variations of CO_2, CH_4 и CO concentrations in the suburb of Saint-Petersburg (Peterhof). *Atmos. Ocean. Opt.* **2019**, *32*, 860–866. https://doi.org/10.15372/AOO20191010. (In Russian).
24. Ionov, D.V.; Poberovskii, A.V. Variability of Nitrogen Oxides in the Atmospheric Surface Layer near Saint Petersburg. *Russ. Meteorol. Hydrol.* **2020**, *45*, 720–726. https://doi.org/10.3103/S1068373920100064.
25. Makarova, M.V.; Alberti, C.; Ionov, D.V.; Hase, F.; Foka, S.C.; Blumenstock, T.; Warneke, T.; Virolainen, Y.A.; Kostsov, V.S.; Frey, M.; et al. Emission Monitoring Mobile Experiment (EMME): An overview and first results of the St. Petersburg megacity campaign 2019. *Atmos. Meas. Tech.* **2021**, *14*, 1047–1073. https://doi.org/10.5194/amt-14-1047-2021.
26. Makarova, M.V.; Kirner, O.; Timofeev, Y.M.; Poberovskii, A.V.; Imkhasin Kh Kh Osipov, S.I.; Makarov, B.K. Analysis of methane total column variations in the atmosphere near St. Petersburg using ground-based measurements and simulations. I*zv. Atmos. Ocean. Phys.* **2015**, *51*, 177–185. https://doi.org/10.1134/S0001433815010089.
27. Makarova, M.V.; Kirner, O.; Timofeev, Y.M.; Poberovskii, A.V.; Imkhasin K.K. Osipov, S.I.; Makarov, B.K. Annual cycle and long-term trend of the methane total column in the atmosphere over the St. Petersburg region. *Izv. Atmos. Ocean. Phys.* **2015**, *51*, 431–438. https://doi.org/10.1134/S0001433815040088.
28. Makarova, M.V.; Poberovskii, A.V.; Polyakov, A.V.; Visheratin, K.N. Time variability of the total methane content in the atmosphere over the vicinity of St. Petersburg. *Izv. Atmos. Ocean. Phys.* **2009**, *45*, 723–730. https://doi.org/10.1134/S000143380906005X.
29. Makarova, M.V.; Poberovskii, A.V.; Osipov, S.I. Time variations of the total CO content in the atmosphere near St. Petersburg. *Izv. Atmos. Ocean. Phys.* **2011**, *47*, 739–746. https://doi.org/10.1134/S0001433811060090.
30. Poberovskii, A.V. High-resolution ground measurements of the IR spectra of solar radiation. *Atmos. Ocean. Opt.* **2010**, *23*, 161–163. https://doi.org/10.1134/S1024856010020132.
31. Hase, F.; Blumenstock, T.; Paton-Walsh, C. Analysis of the instrumental line shape of high-resolution Fourier transform IR spectrometers with gas cell measurements and new retrieval software. *Appl. Opt.* **1999**, *38*, 3417–3422. https://doi.org/10.1364/AO.38.003417.
32. Tikhonov, A. On the solution of incorrectly stated problems and a method of regularization. *Dokl. Acad. Nauk SSSR* **1963**, *151*, 501–504.
33. Rodgers, C.D. Retrieval of atmospheric temperature and composition from remote measurements of thermal radiation. *Rev. Geophys.* **1976**, *14*, 609–624. https://doi.org/10.1029/RG014i004p00609.
34. Rodgers, C.D. *Inverse Methods for Atmospheric Sounding: Theory and Practice, Series on Atmospheric, Oceanic and Planetary Physics*; World Scientific Publishing Co.: Singapore, 2000; Volume 2, p. 256, ISBN 978-981-02-2740-1. https://doi.org/10.1142/3171.
35. Pougatchev, N.S.; Connor, B.J.; Rinsland, C.P. Infrared measurements of the ozone vertical distribution above Kitt Peak. *J. Geophys. Res.* **1995**, *100*, 16689–16697.
36. Rinsland, C.P.; Jones, N.B.; Connor, B.J.; Logan, J.A.; Pougatchev NSGoldman, A.; Murcray, F.J.; Stephen, T.M.; Pine, A.S.; Zander, R.; Mahieu, E.; et al. Northern and southern hemisphere ground-based infrared spectroscopic measurements of tropospheric carbon monoxide and ethane. *J. Geophys. Res.* **1998**, *103*, 28197–28217. https://doi.org/10.1029/98JD02515.
37. Hase, F.; Hannigan, J.W.; Coffey, M.T.; Goldman, A.; Höpfner, M.; Jones, N.B.; Rinsland, C.P.; Wood, S.W. Intercomparison of retrieval codes used for the analysis of high-resolution, ground-based FTIR measurements. *J. Quant. Spectros. Radiat. Transf.* **2004**, *87*, 25–52.
38. Hase, F.; Demoulin, P.; Sauval, A.J.; Toon, G.C.; Bernath, P.F.; Goldman, A.; Hannigan, J.W.; Rinsland, C.P. An empirical line-by-line model for the infrared solar transmittance spectrum from 700 to 5000 cm^{-1}. *J. Quant. Spectros. Radiat. Transf.* **2006**, *102*, 450–463.
39. Sussmann, R.; Forster, F.; Rettinger, M.; Jones, N. Strategy for high-accuracy-and-precision retrieval of atmospheric methane from the mid-infrared FTIR network. *Atmos. Meas. Tech.* **2011**, *4*, 1943–1964. https://doi.org/10.5194/amt-4-1943-2011.
40. García, O.E.; Schneider, M.; Sepúlveda, E.; Hase, F.; Blumenstock, T.; Cuevas, E.; Ramos, R.; Gross, J.; Barthlott, S.; Röhling, A.N.; et al. Twenty years of ground-based NDACC FTIR spectrometry at Izaña Observatory—Overview and long-term comparison to other techniques. *Atmos. Chem. Phys.* **2021**, *21*, 15519–15554. https://doi.org/10.5194/acp-21-15519-2021.

41. Steck, T. Methods for determining regularization for atmospheric retrieval problems. *Appl. Opt.* **2002**, *41*, 1788–1797. https://doi.org/10.1364/AO.41.001788.
42. Vigouroux, C.; Bauer Aquino, C.A.; Bauwens, M.; Becker, C.; Blumenstock, T.; De Mazière, M.; García, O.; Grutter, M.; Guarin, C.; Hannigan, J.; et al. NDACC harmonized formaldehyde time series from 21 FTIR stations covering a wide range of column abundances. *Atmos. Meas. Tech.* **2018**, *11*, 5049–5073. https://doi.org/10.5194/amt-11-5049-2018.
43. IRWG, Uniform Retrieval Parameter Summary. 2022. Available online: https://www.acom.ucar.edu/irwg/IRWG_Uniform_RP_Summary-3.pdf (accessed on 24 October 2023).
44. Barthlott, S.; Schneider, M.; Hase, F.; Wiegele, A.; Christner, E.; González, Y.; Blumenstock, T.; Dohe, S.; García, O.E.; Sepúlveda, E.; et al. Using XCO_2 retrievals for assessing the long-term consistency of NDACC/FTIR data sets. *Atmos. Meas. Tech.* **2015**, *8*, 1555–1573. https://doi.org/10.5194/amt-8-1555-2015.
45. Garcia, R.R.; Marsh, D.R.; Kinnison, D.E.; Boville, B.A.; Sassi, F. Simulation of secular trends in the middle atmosphere, 1950-2003. *J. Geophys. Res.* **2007**, *112*, D09301. https://doi.org/10.1029/2006JD007485.
46. Rothman, L.S.; Jacquemart, D.; Barbe, A.; Benner, D.C.; Birk, M.; Brown, L.R.; Carleer, M.R.; Chackerian, C.; Chance, K.; Coudert, L.H.; et al. The HITRAN 2004 molecular spectroscopic database. *J. Quant. Spectrosc. Radiat. Transf.* **2005**, *96*, 139–204.
47. Rothman, L.S.; Gordon, I.E.; Barbe, A.; Benner, D.C.; Bernath, P.F.; Birk, M.; Boudon, V.; Brown, L.R.; Campargue, A.; Champion, J.-P.; et al. The Hitran 2008 molecular spectroscopic database. *J. Quant. Spectrosc. Radiat. Transf.* **2009**, *110*, 533–572.
48. Rothman, L.S.; Gordon, I.E.; Babikov, Y.; Barbe, A.; Benner, D.C.; Bernath, P.F.; Birk, M.; Bizzocchi, L.; Boudon, V.; Brown, L.R.; et al. The HITRAN2012 molecular spectroscopic database. *J. Quant. Spectrosc. Radiat. Transf.* **2013**, *130*, 4–50. https://doi.org/10.1016/j.jqsrt.2013.07.002.
49. Gordon, I.E.; Rothman, L.S.; Hill, C.; Kochanov, R.V.; Tan, Y.; Bernath, P.F.; Birk, M.; Boudon, V.; Campargue, A.; Chance, K.V.; et al. The HITRAN2016 molecular spectroscopic database. *J. Quant. Spectrosc. Radiat. Transf.* **2017**, *203*, 3–69. https://doi.org/10.1016/j.jqsrt.2017.06.038.
50. Toon, G.C.; Blavier, J.F.; Sung, K.; Rothman, L.S.; Gordon, I.E. HITRAN spectroscopy evaluation using solar occultation FTIR spectra. *J. Quant. Spectrosc. Radiat. Transf.* **2016**, *182*, 324–336. https://doi.org/10.1016/j.jqsrt.2016.05.021.
51. Hase, F.; Wallace, L.; McLeod, S.D.; Harrison, J.J.; Bernath, P.F. The ACE-FTS atlas of the infrared solar spectrum. *J. Quant. Spectros. Radiat. Transf.* **2010**, *111*, 521–528.
52. Vigouroux, C.; Stavrakou, T.; Whaley, C.; Dils, B.; Duflot, V.; Hermans, C.; Kumps, N.; Metzger, J.-M.; Scolas, F.; Vanhaelewyn, G.; et al. FTIR time-series of biomass burning products (HCN, C_2H6, C_2H_2, CH_3OH, and HCOOH) at Reunion Island (21° S, 55° E) and comparisons with model data, *Atmos. Chem. Phys.* **2012**, *12*, 10367–10385. https://doi.org/10.5194/acp-12-10367-2012.
53. Viatte, C.; Strong, K.; Walker, K.A.; Drummond, J.R. Five years of CO, HCN, C_2H_6, C_2H_2, CH_3OH, HCOOH and H_2CO total columns measured in the Canadian high Arctic. *Atmos. Meas. Tech.* **2014**, *7*, 1547–1570. https://doi.org/10.5194/amt-7-1547-2014.
54. Hannigan, J.W.; Ortega, I.; Shams, S.B.; Blumenstock, T.; Campbell, J.E.; Conway, S.; Flood, V.; Garcia, O.; Griffith, D.; Grutter, M.; et al. Global atmospheric OCS trend analysis from 22 NDACC stations. *J. Geophys. Res. Atmos.* **2022**, *127*, e2021JD035764. https://doi.org/10.1029/2021JD035764.
55. Vigouroux, C.; De Mazière, M.; Demoulin, P.; Servais, C.; Hase, F.; Blumenstock, T.; Kramer, I.; Schneider, M.; Mellqvist, J.; Strandberg, A.; et al. Evaluation of tropospheric and stratospheric ozone trends over Western Europe from ground-based FTIR network observations. *Atmos. Chem. Phys.* **2008**, *8*, 6865–6886. https://doi.org/10.5194/acp-8-6865-2008.
56. Deutscher, N.M.; Griffith, D.W.T.; Bryant, G.W.; Wennberg, P.O.; Toon, G.C.; Washenfelder, R.A.; Keppel-Aleks, G.; Wunch, D.; Yavin, Y.; Allen, N.T.; et al. Total column CO_2 measurements at Darwin, Australia—Site de-scription and calibration against in situ aircraft profiles. *Atmos. Meas. Tech.* **2010**, *3*, 947–958. https://doi.org/10.5194/amt-3-947-2010.
57. Lomb, N.R. Least-squares frequency analysis of unequally spaced data. *Astrophys. Space Sci.* **1976**, *39*, 447–462. https://doi.org/10.1007/BF00648343.
58. VanderPlas, J.T. Understanding the Lomb–Scargle Periodogram. *Astrophys. J. Suppl. Ser.* **2018**, *236*, 16. https://doi.org/10.3847/1538-4365/aab766.
59. The Astropy Collaboration. The Astropy Project: Sustaining and Growing a Community-oriented Open-sourceProject and the Latest Major Release(v5.0)of the Core Package. *Astrophys. J.* **2022**, *935*, 20. https://doi.org/10.3847/1538-4357/ac7c74.
60. Efron, B.; Tibshirani, R.J. *An Introduction to the Bootstrap*; CRC Press: Boca Raton, FL, USA, 1994.
61. Yamanouchi, S.; Strong, K.; Colebatch, O.; Conway, S.; Jones DB, A.; Lutsch, E.; Roche, S. Atmospheric trace gas trends obtained from FTIR column measurements in Toronto, Canada from 2002–2019. *Environ. Res. Commun.* **2021**, *3*, 051002. https://doi.org/10.1088/2515-7620/abfa65.
62. Jöckel, P.; Tost, H.; Pozzer, A.; Bruhl, C.; Buchholz, J.; Ganzeveld, L.; Hoor, P.; Kerkweg, A.; Lawrence, M.G.; Sander, R.; et al. The atmospheric chemistry general circulation model ECHAM5/MESSy1: Consistent simulation of ozone from the surface to the mesosphere. *Atmos. Chem. Phys.* **2006**, *6*, 5067–5104. https://doi.org/10.5194/acp-6-5067-2006.
63. Kirner, O.; Ruhnke, R.; Buchholz-Dietsch, J.; Jöckel, P.; Brühl, C.; Steil, B. Simulation of polar stratospheric clouds in the chemistry-climate-model EMAC via the submodel PSC. *Geosci. Model Dev.* **2011**, *4*, 169–182. https://doi.org/10.5194/gmd-4-169-2011.
64. Rodgers, C.D.; Connor, B.J. Intercomparison of remotesounding instruments. *J. Geophys. Res.* **2003**, *108*, 4116–4129. https://doi.org/10.1029/2002JD002299.
65. Foka, S.C.; Makarova, M.V.; Poberovsky, A.V.; Ionov, D.V.; Abakumov, E.V. Analysis of mixing ratios of carbon-containing gases at the atmospheric monitoring station of St. Petersburg State University. *Atmos. Ocean. Opt.* **2023**, *36*, 934–941. https://doi.org/10.15372/AOO20231109. (In Russian).

66. Lan, X.; Thoning, K.W.; Dlugokencky, E.J. Trends in globally-averaged CH_4, N_2O, and SF6 determined from NOAA Global Monitoring Laboratory measurements. Version 2023-10. https://doi.org/10.15138/P8XG-AA10